Heliyon 7 (2021) e06622

Contents lists available at ScienceDirect

Heliyon

journal homepage: www.cell.com/heliyon

Research article

Highly efficient synthesis of biodiesel catalyzed by a cellulose@hematite-zirconia nanocomposite

Helmiyati Helmiyati *, Yuni Budiman, Gusma Harfiana Abbas, Fitriyah Wulan Dini, Munawar Khalil

Department of Chemistry, Faculty of Mathematic and Natural Sciences, Universitas Indonesia, 16424 Depok, West Java, Indonesia

ARTICLE INFO

Keywords:
Biodiesel
Cellulose
Heterogeneous catalyst
Lauric acid
Rice straw

ABSTRACT

The depletion of fossil fuels calls for the development of renewable alternatives such as biodiesel and has inspired much research on catalysts for the production of biodiesel through the esterification of biomass-derived materials. Herein, a green heterogeneous catalyst for highly efficient biodiesel synthesis was fabricated from rice straw–derived cellulose, hematite, and zirconia and was shown to contain porous irregularly shaped α-Fe_2O_3–ZrO_2 composites (average particle size = 42.5 nm) evenly distributed on the nanocellulose surface. The optimal catalyst (nanocellulose:α-Fe_2O_3–ZrO_2 = 2:1, w/w) afforded biodiesel in a yield of 92.50% and with specifications close to those prescribed by international standards. This catalyst could be reused for up to five cycles without a marked activity loss, with the biodiesel yield in the fifth cycle equaling 80.0%. The developed nanocomposite holds great promise for cutting the costs of biodiesel production, as it is derived from biodegradable raw materials and is renewable, non-corrosive, easy to handle, and green. In addition, the large-scale discharge of this catalyst after use does not pose a hazard to the environment.

1. Introduction

Inexpensive modified lignocellulosic materials hold great promise for the development of biopolymer-based catalysts [1]. Biomass-derived biopolymers play an important role in the mitigation of fossil fuel depletion and global warming caused by the use of synthetic polymers [2, 3]. As a representative sustainable biopolymer, cellulose features high natural abundance, belonging to the green support group [3, 4], and can be isolated from rice straw (among other sources), which is an abundant, cheap, and green material that is generated in large quantities as a byproduct of rice production [5, 6] and has a high cellulose content [7, 8].

Rice straw is often disposed of by burning, however, causes serious environmental pollution when performed in the open air [9]. Therefore, the usage of rice straw as a source of cellulose allows one to reduce the environmental impact of rice straw, improve the overall economy [10], conserve natural resources, and mitigate the health problems associated with air pollution due to rice straw burning [11].

The β-1,4-glycosidic bonds of cellulose make it a durable support for the formation of catalytically active nanocomposites with inorganic substances [12]. Nanocomposites produced from nanopolymers and inorganic nanoparticles offer the advantages of natural abundance and biodegradability, often benefitting from the synergy between their components [13], as exemplified by the numerous synthetic applications of cellulose-based catalysts (e.g., Pd/cellulose nanocomposites [14], γ-Fe_2O_3/Cu@cellulose [15], magnetic nanocellulose [13], cellulose/ZrO_2 [16] and cellulose@Fe_2O_3 [17]

The depletion of crude oil resources has encouraged research on the production of renewable fuels such as biodiesel [18, 19] which can be obtained from renewable sources such as edible vegetable oils, inedible oils, and animal fats [20] through catalytic triglyceride transesterification and free fatty acid esterification and offers the advantages of renewability, reduction of greenhouse gas emissions, biodegradability, and non-toxicity [21, 22, 23, 24].

Indonesia has a great opportunity to convert agricultural biomass such as coconuts, corn, peanuts, cassava, and palm oil into renewable energy sources. In particular, coconut oil is well suited for biodiesel production, as it is rich in fatty acids, cheap, and readily available in Indonesia [25].

Several catalysts with nanocellulose as a support and inorganic compounds as active ingredients have been synthesized for biodiesel production [26, 27] Nonetheless, very few studies have evaluated the effect of nanocellulose supports on the catalytic activities of nanohematite and

* Corresponding author.
E-mail address: helmiyati@sci.ui.ac.id (H. Helmiyati).

https://doi.org/10.1016/j.heliyon.2021.e06622
Received 29 November 2020; Received in revised form 25 January 2021; Accepted 24 March 2021

nanozirconia. To bridge this gap, the present study probes the effect of nanocellulose loading on the performance of cellulose@ α-Fe_2O_3–ZrO_2 nanocomposites for biodiesel production from lauric acid.

2. Materials and methods

2.1. Materials

Rice straw was sourced from Central Java, Indonesia. $FeCl_2{\cdot}4H_2O$ and $FeCl_3{\cdot}6H_2O$ as nano-α-Fe_2O_3 precursors, $ZrOCl_2{\cdot}8H_2O$ as a nano-ZrO_2 precursor, and H_2SO_4 used for nanocellulose synthesis were procured from Merck, and lauric acid was isolated from locally produced coconut oil.

2.2. Synthesis of nanocellulose from rice straw

Cellulose was isolated from rice straw as described in our previous study [28]and converted into nanocellulose by 2 h ultrasonication-assisted hydrolysis in 65 wt.% H_2SO_4 at 45 °C [29]. The obtained nanocellulose precipitate was washed with water to neutral pH, centrifuged for 15 min, dried, and characterized by Fourier transform infrared (FTIR) spectroscopy, X-ray diffraction (XRD), Brunauer–Emmett–Teller (BET), and scanning electron microscopy (SEM).

2.3. Synthesis of nano-α-Fe_2O_3

Nano-α-Fe_2O_3 was prepared using a slight modification of a previously reported method [30]. $FeCl_2{\cdot}4H_2O$ and $FeCl_3{\cdot}6H_2O$ were separately dissolved in distilled water to concentrations of 2 M and 1 M, respectively, and the respective solutions were mixed in a 2:3 (v/v) ratio. The mixture was slowly supplemented with 2 M NH_4OH to reach a pH of 10 and vigorously stirred for 2 h. The brown precipitate was separated, rinsed with distilled water and ethanol, dried at 60 °C overnight, and calcined at 600 °C for 1 h.

2.4. Synthesis of nano-ZrO_2

Nano-ZrO_2 was prepared using a slight modification of a previously reported method [31]. A 1 M solution of $ZrOCl_2{\cdot}8H_2O$ was slowly treated with 2 M NaOH to reach a pH of 10, and the mixture was stirred for 15 min. The white precipitate was separated, sequentially rinsed with water and acetone, dried at 60 °C, and calcined at 700 °C for 1 h.

2.5. Synthesis of cellulose@α-Fe_2O_3–ZrO_2 nanocomposites

The first stage, α-Fe_2O_3–ZrO_2 composites were prepared as described elsewhere [32]. Briefly, α-Fe_2O_3 was added to a solution containing H_2O, ethanol, and ammonia, and the mixture was ultrasonicated to form a homogeneous suspension. The resulting dispersion was slowly supplemented with $ZrOCl_2{\cdot}8H_2O$ and stirred for 6 h. The precipitate was separated, sequentially rinsed with ethanol and water, and oven-dried at 60 °C for 12 h to afford α-Fe_2O_3–ZrO_2. In the second stage, cellulose@α-Fe_2O_3–ZrO_2 nanocomposites were prepared using a slight modification of a previously reported method [33]. Briefly, nanocellulose was homogenously dispersed in an aqueous solution of NaOH and urea at −4 °C, the solution was supplemented with a dispersion of α-Fe_2O_3–ZrO_2 in aqueous NaOH, and the resulting mixture was stirred for 6 h. The product was separated, sequentially rinsed with ethanol and water, and dried. The resulting cellulose@α-Fe_2O_3–ZrO_2 nanocomposites were characterized by FTIR, XRD, BET, SEM, and transmission electron microscopy (TEM).

2.6. Catalytic activity assessment

Catalytic activity was evaluated in terms of the ability to promote the esterification of lauric acid, the major fatty acid (52.68%) of coconut oil [34], with methanol, as described in previous studies [35, 36, 37]. Herein, we varied the nanocellulose: α-Fe_2O_3–ZrO_2 mass ratio (0.5:1, 1:1, 2:1, 3:1) and catalyst type (nano-α-Fe_2O_3, nano-ZrO_2, α-Fe_2O_3–ZrO_2, and cellulose@α-Fe_2O_3–ZrO_2). Biodiesel yield was calculated as Eq. (1) [36]:

$$Biodiesel\ yield\ (\%) = \frac{Weight\ of\ biodiesel}{Weight\ of\ lauric\ acid} \times 100\ \% \quad (1)$$

2.7. Determination of biodiesel properties

Biodiesel parameters, such as acid number (AN), cetane number (CN), American petroleum institute (API), higher heating value (HHV) were calculated as Eqs. (2), (3), (4), and (5) [38, 39]:

$$\mathrm{AN} = \frac{V_{KOH} \times N_{KOH} \times 56.1}{W} \quad (2)$$

$$\mathrm{CN} = 46.3 + \frac{5458}{\mathrm{SN}} - 0.225 \times \mathrm{IN} \quad (3)$$

$$\mathrm{API} = \frac{141.5}{\text{Specific gravity}} - 131.5 \quad (4)$$

$$\mathrm{HHV}\left(\frac{\mathrm{MJ}}{\mathrm{kg}}\right) = 49.43 - [0.041(\mathrm{SN}) + 0.015(\mathrm{IN})] \quad (5)$$

The saponification number (SN) and the iodine number (IN) were calculated as Eqs. (6) and (7) [40]:

$$\mathrm{SN} = \frac{V_{HCL} \times N_{HCL} \times 56.1}{W} \quad (6)$$

$$\mathrm{IN} = \frac{(V_{Na_2S_2O_3}blank - V_{Na_2S_2O_3}sample)\, N_{Na_2S_2O_3} \times 12.69}{W} \quad (7)$$

2.8. Reusability of catalysts

The reusability of cellulose@α-Fe_2O_3–ZrO_2 nanocomposites were observed using a slight modification of a previously reported method [41]. The catalyst was separated and washed several times with hot ethanol and then hexane to remove the residual of lauric acid and product which adsorbed on the catalyst surface, and then dried in an oven at 100 °C for 12 h. To observe the leaching of the catalyst species into the reaction medium causes contamination of the final product and so lead to a decrease in catalyst activity [42]We tested the nanocomposite weight of reused catalysts after each cycle were measured by gravimetry to confirm the quantity of catalyst leached and to confirm the catalytic system behave a heterogeneous.

3. Results and discussion

3.1. Formation of cellulose@α-Fe_2O_3–ZrO_2 nanocomposites

Rice straw cellulose was activated by hydrolysis under strongly acidic conditions to increase the active group content, surface area, and catalytic efficiency. This hydrolysis resulted in the cleavage of glycoside bonds to form nanocellulose sulfonates, which, in turn, were hybridized with α-Fe_2O_3–ZrO_2 to form cellulose@α-Fe_2O_3–ZrO_2 nanocomposites (Figure 1).

3.2. Characterization

3.2.1. FTIR analysis

Figure 2 shows the results of FTIR analysis. The spectrum of nanocellulose (Figure 2a) featured an O–H stretch at 3250–3500 cm^{-1}, a C–H stretch at 2940 cm^{-1}, and absorption bands of β-glycoside bonds at 1678, 1055, and 930 cm^{-1} characteristic of cellulose [13]. The bands at 1140

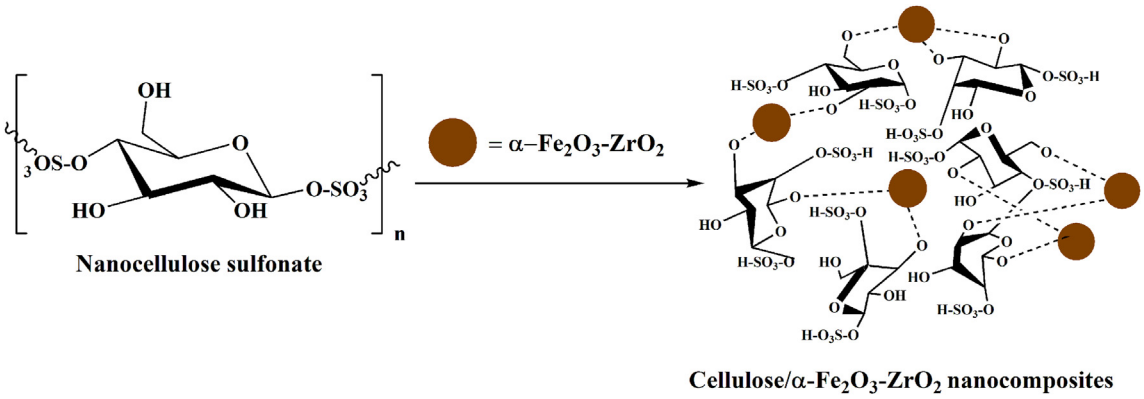

Figure 1. Proposed scheme of cellulose@α-Fe_2O_3–ZrO_2 nanocomposites formation.

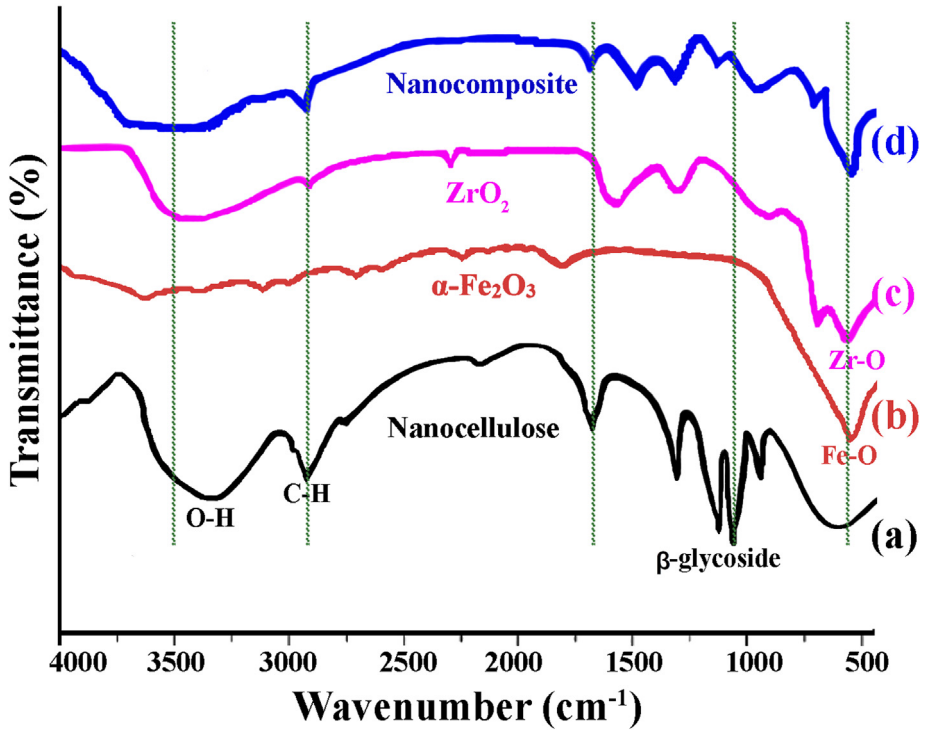

Figure 2. FTIR spectra of (a) nanocellulose, (b) α-Fe_2O_3, (c) ZrO_2 and (d) cellulose@α-Fe_2O_3–ZrO_2.

and 1310 cm^{-1} were assigned to the symmetric vibration of SO_3^-, the symmetric vibration of the O=S=O unit in the SO_3H group, and the asymmetric vibration of SO_2^-, respectively, and indicated the successful formation of nanocellulose sulfonates. The spectra of α-Fe_2O_3 (Figure 2b) and ZrO_2 (Figure 2c) featured peaks at 543 cm^{-1} (Fe–O) [43, 44]and 540 cm^{-1} (Zr–O) [45], respectively. The spectrum of cellulose@α-Fe_2O_3–ZrO_2 (Figure 2d) featured a band at 530 cm^{-1} that corresponded to the overlap of Fe–O and Zr–O peaks. The observation of this band, together with the sloping nature and position shift of the typical peaks of β-glycosidic bonds, SO_3^- bonds, and O–H bonds indicated the successful hybridization of nanocellulose with α-Fe_2O_3–ZrO_2.

3.2.2. XRD analysis

The XRD pattern of nanocellulose (Figure 3a) featured peaks at 2θ = 16°, 22° (most intense), and 35°, corresponding to reflections from the (101), (002), and (040) planes [46], respectively. These data were in line with the results of our previous studies [13, 27, 43]. The diffraction pattern of α-Fe_2O_3 (Figure 3b) featured peaks at 2θ = 25.3°, 33.5°, 36.3°, 40.3°, 50.2°, 55.2°, 57.8°, 63.5°, 65.2°, and corresponding to the (012), (104), (110), (113), (024), (116), (122), (214), and (300) planes of Fe_2O_3, respectively. The strongest peaks were assigned to the (104) and (110) planes, in line with the results of our previous study [44, 47]. The diffraction pattern of nano-ZrO_2 (Figure 3c) featured peaks of the monoclinic (2θ = 24.5°, 28.0°, 31.0°, and 34.0°) and tetragonal (2θ = 35.0°, 50.0°, and 60.0°) forms [45]. The pattern of cellulose@α-Fe_2O_3–ZrO_2 (Figure 3d) showed the peaks of the above three constituents, and the shift of α-Fe_2O_3 and ZrO_2 peaks indicated that these oxides were bonded to nanocellulose, in line with the results of FTIR analysis. The average crystallite size was calculated using Debye-Scherrer equation [24] was obtained as 40.5 nm.

3.2.3. BET

The N_2 sorption isotherms of nanocellulose and after loading hematite and zirconia as cellulose@α-Fe_2O_3–ZrO_2 (Figure 4) displayed a typical type IV isotherm denoting the existence of mesopores for pores with diameters in the range 2–50 nm [48]. Figure 4 featured the resulted

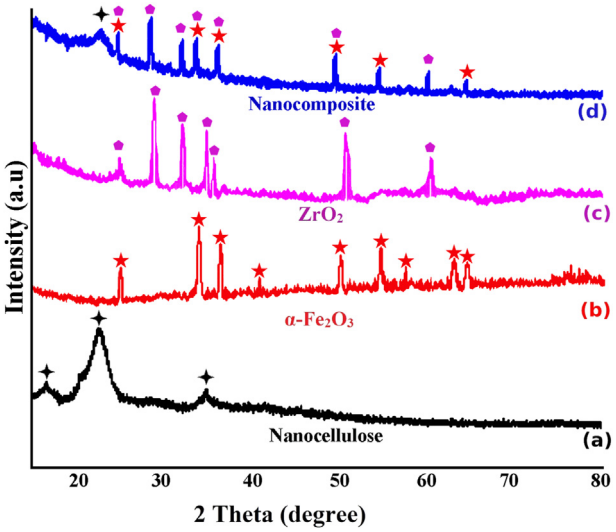

Figure 3. XRD patterns of (a) nanocellulose, (b) α-Fe_2O_3, (c) ZrO_2 and (d) cellulose@α-Fe_2O_3–ZrO_2 (c).

from the BET surface area and pore volume for nanocellulose and nanocomposite reveal cellulose@α-Fe_2O_3–ZrO_2 a higher BET surface area (852 m^2g^{-1}) and pore volume (0.85 cm^3g^{-1}) than nanocellulose (720 m^2g^{-1}, 0.52 cm^3g^{-1}). The pore size of nanocellulose and cellulose@α-Fe_2O_3–ZrO_2 were 24 and 13 nm, respectively, and indicated that composite of α-Fe_2O_3–ZrO_2 had embedded on the pore surface of nanocellulose.

3.2.4. SEM

Surface morphology was probed by SEM. Nanocellulose comprised fibers with a smooth, uniform, and homogeneous surface (Figure 5a), which agreed with the results of previous studie [35]. α-Fe_2O_3 comprised hexagonal particles (Figure 5b), whereas ZrO_2 (Figure 5c) featured particles of diverse shapes (e.g., spherical, elliptical, and angular), which suggested the monoclinic structure of the latter oxide, in line with XRD data. Cellulose@α-Fe_2O_3–ZrO_2 particles had an uneven surface (Figure 5d), and the distribution of α-Fe_2O_3–ZrO_2 on the nanocellulose surface was observed by elemental mapping (Figure 6).

Figure 6a–d show that the constituent elements were evenly distributed on the cellulose@α-Fe_2O_3–ZrO_2 surface, and α-Fe_2O_3–ZrO_2 was also evenly distributed on the nanocellulose surface, which confirmed the successful synthesis of the nanocellulose-supported catalyst.

3.2.5. TEM

Nanocomposite structure was probed by TEM. Low-resolution TEM imaging (Figure 7a) revealed that the catalyst particles had an irregular shape, with dark hexagonal and spherical particles corresponding to the α-Fe_2O_3–ZrO_2 composite (red circle). The average size of α-Fe_2O_3–ZrO_2 particles was determined as 42.5 nm and cylindrical particles corresponding to nanocellulose fiber (blue circle). Figure 7b–d present high-resolution TEM images of the porous cellulose@α-Fe_2O_3–ZrO_2 nanocomposite.

3.3. Catalytic activity of cellulose@α-Fe_2O_3–ZrO_2

Catalytic activity for the conversion of lauric acid into biodiesel was probed for 3 h at 60 °C using a lauric acid amount of 10 g, a methanol:lauric acid molar ratio of 12:1, and a catalyst loading of 2 wt.%.

3.3.1. Effect of nanocellulose: α-Fe_2O_3–ZrO_2 mass ratio on biodiesel yield

The fibrous and porous structure of nanocellulose allowed α-Fe_2O_3–ZrO_2 to be embedded and evenly spread on the pore surface,

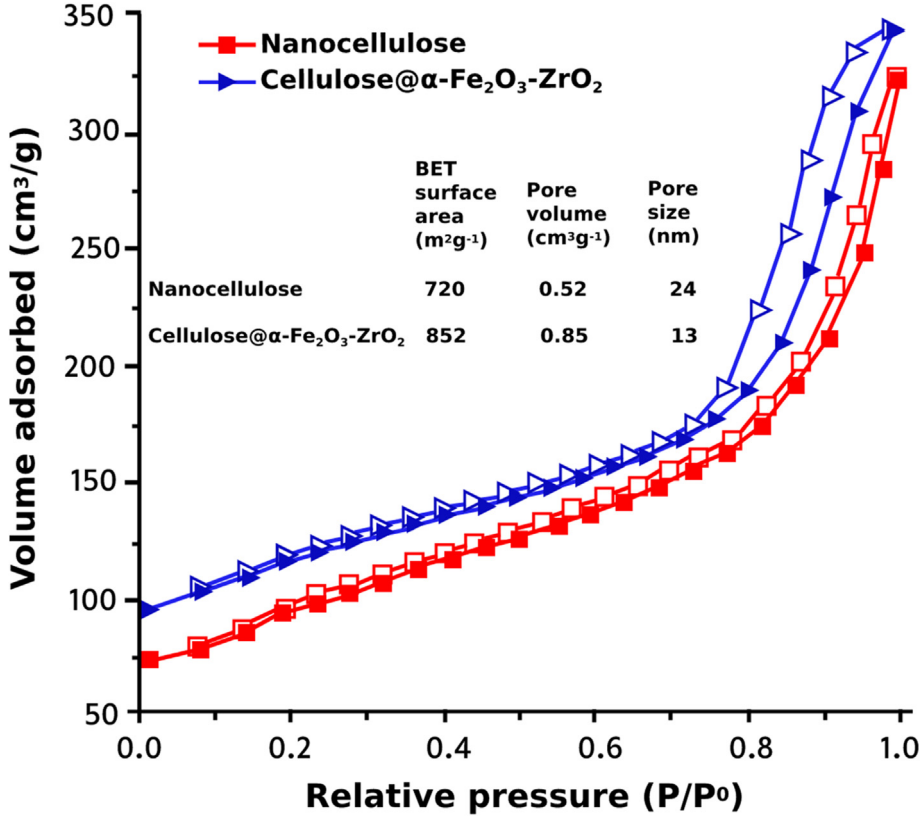

Figure 4. N_2 sorption isotherms curves of nanocellulose and cellulose@α-Fe_2O_3–ZrO_2.

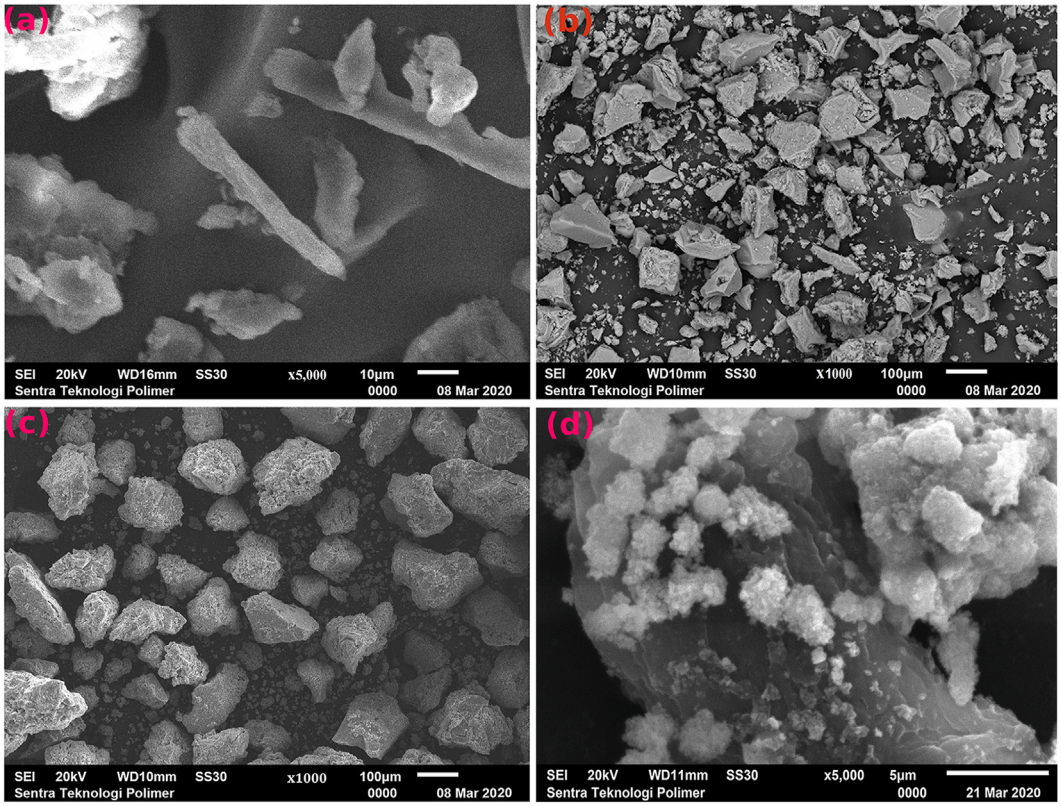

Figure 5. SEM images of (a) nanocellulose, (b) α-Fe_2O_3, (c) ZrO_2, (d) and cellulose@α-Fe_2O_3–ZrO_2.

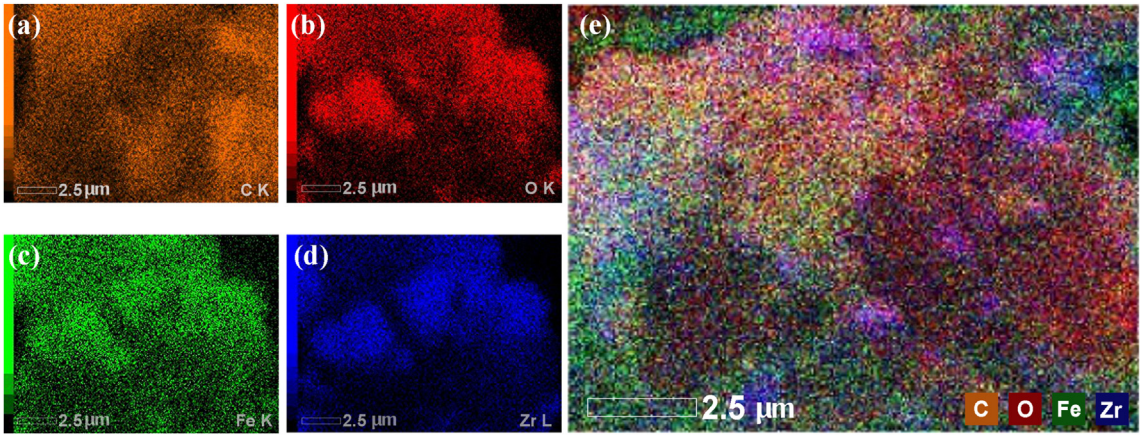

Figure 6. Elemental distribution mappings [(a) C, (b) O, (c) Fe, (d) Zr and (e) overall element] of cellulose@α-Fe_2O_3–ZrO_2.

which resulted in enhanced catalytic activity. Herein, we investigated the effect of the nanocellulose: α-Fe_2O_3–ZrO_2 mass ratio (*r*) on (i) biodiesel yield after 3 h, (ii) the highest attainable biodiesel yield, and (iii) the time needed to obtain this maximal yield (Figure 8). At a fixed reaction time of 3 h with the bar chart in grey color, the yield increased with increasing r, equaling 35.00, 70.50, 92.50, and 92.50% at r = 0.5:1, 1:1, 2:1, and 3:1, respectively. This shows that at r = 2:1, all nanocellulose pores were filled with α-Fe_2O_3 and ZrO_2 nanoparticles as active sites, which resulted in efficient biodiesel production. To observe the mass ratio effect to the reaction rate by extending the time indicated by a black bar chart and red line is the reaction time so that the perfect reaction is achieved. When the reaction time was extended, the maximal yields for r = 0.5:1, 1:1, 2:1, and 3:1, equaling 90,00, 90.50, 92.50 and 92.50%, respectively. Therefore, the catalyst with r = 2:1 was concluded to be optimal condition for this esterification reaction.

3.3.2. *Effect of catalyst type on biodiesel yield*

Next, we probed the effect of catalyst type on (i) biodiesel yield after 3 h, (ii) the highest attainable biodiesel yield, and (iii) the time needed to obtain this maximal yield (Figure 9). At a fixed time of 3 h with the bar chart in dark blue color, α-Fe_2O_3, ZrO_2, α-Fe_2O_3–ZrO_2, and cellulose@α-Fe_2O_3–ZrO_2 (*r* = 2:1) achieved yields of 30.00, 51.50, 86.80, and 92.50%, respectively. The fact that pure ZrO_2 achieved a greater yield than α-Fe_2O_3 means that the former oxide provided more important active sites than α-Fe_2O_3. The fact that the highest yield was observed for cellulose@α-Fe_2O_3–ZrO_2 was ascribed to the synergetic effects arising upon the hybridization of the biopolymer with inorganic nanoparticles [13]. Furthermore, we also observed the effect of catalyst type to the reaction rate by extending the time indicated by light green the bar chart and red line is the reaction time so that the perfect reaction is achieved. When the reaction time was extended, α-Fe_2O_3, ZrO_2, α-Fe_2O_3–ZrO_2, and

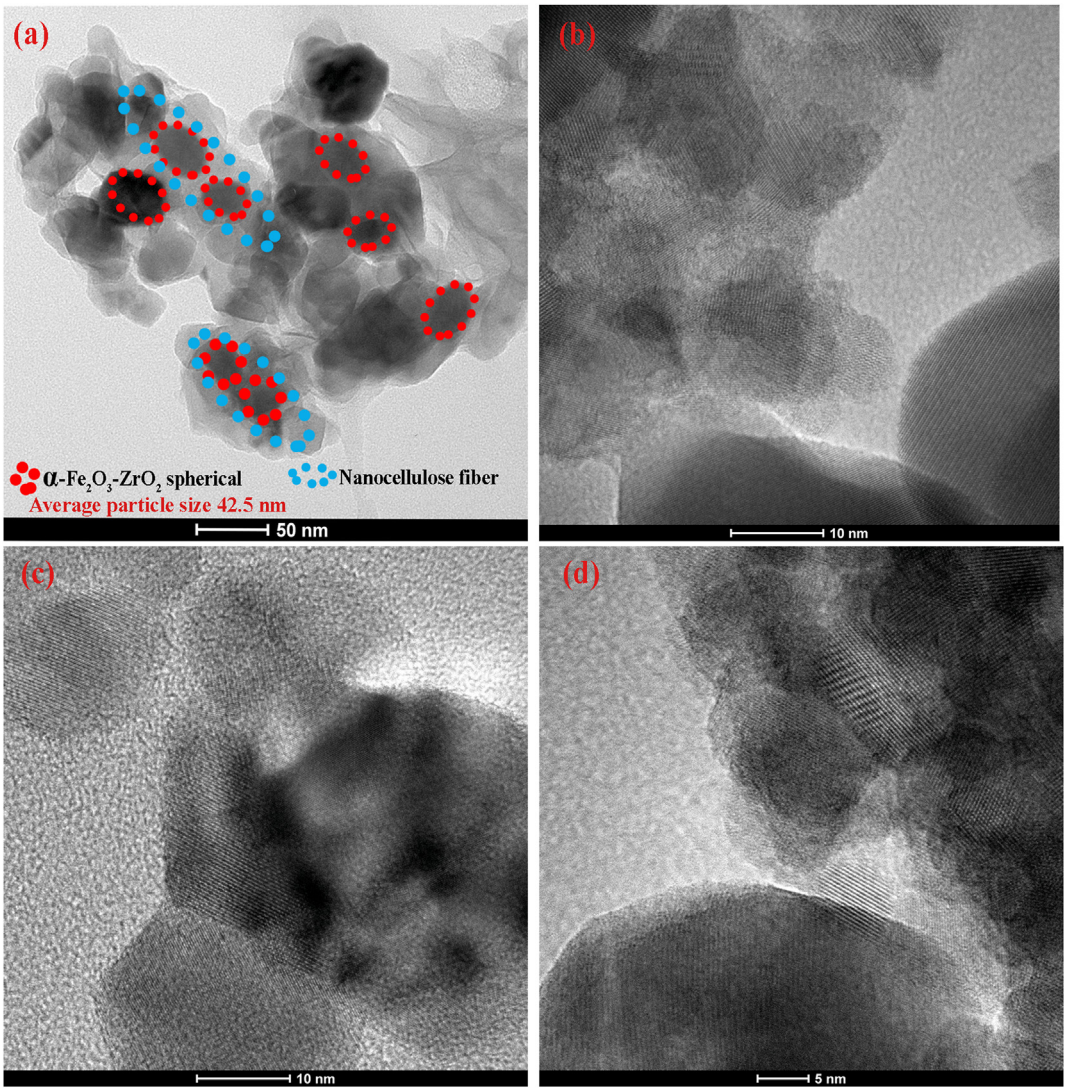

Figure 7. TEM image [(a) 50 nm, (b) 10 nm, (c) 10 nm and (d) 5 nm scale] of cellulose@α-Fe_2O_3–ZrO_2.

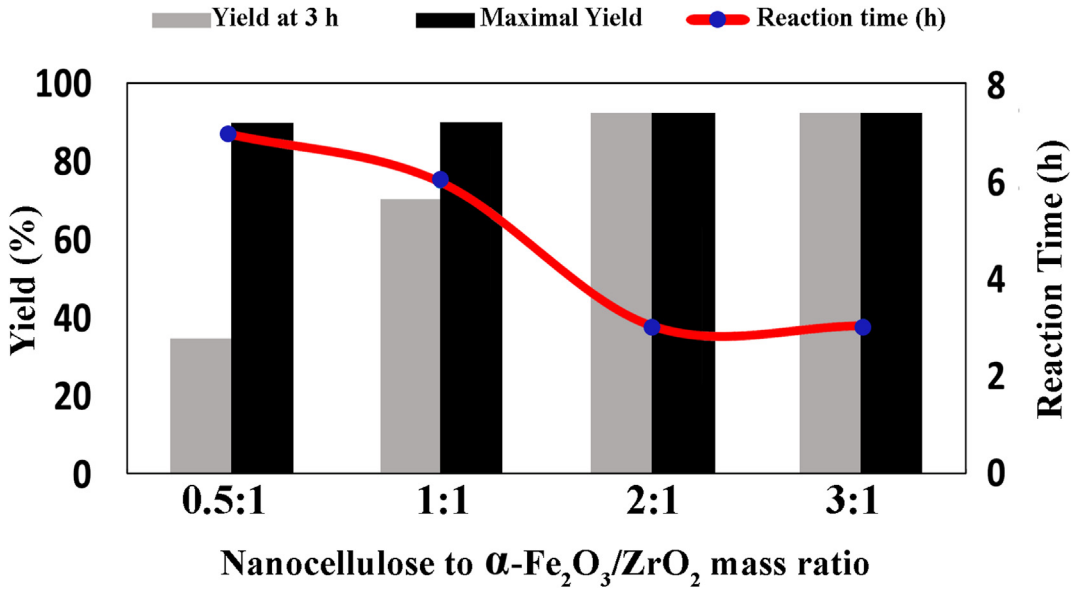

Figure 8. Effect of nanocellulose to α-Fe_2O_3–ZrO_2 mass ratio on percent yield and reaction time.

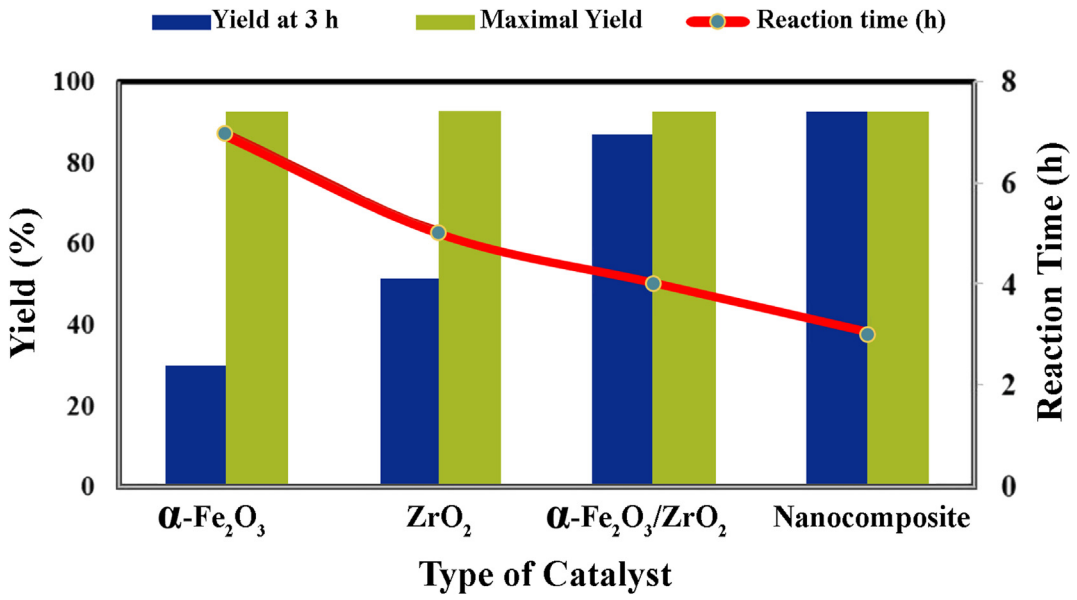

Figure 9. Effect of type catalyst on percent yield and reaction time.

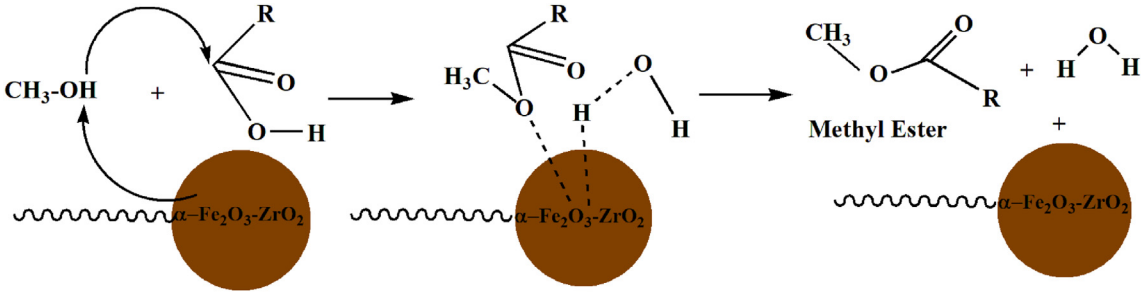

Figure 10. Proposed reaction mechanism for the esterification of lauric acid over the cellulose@α-Fe_2O_3–ZrO_2 catalyst.

cellulose@α-Fe_2O_3–ZrO_2 achieved maximal yields of 92.50% after 7, 5, 4, and 3 h, respectively. Therefore, the cellulose@α-Fe_2O_3–ZrO_2 nanocomposite is the best suited for the studied esterification reaction, owing to the existence of both acidic and basic sites, besides the presence of pores and large BET surface area (Figure 4) to accommodate the reactants and activate the reaction. Briefly, our explanation for the catalytic activity of the cellulose@α-Fe_2O_3–ZrO_2 catalyst in the reaction by eliminating protons from methanols which attacked the carboxylic group of acids to form an activated complex which is adsorbed on the surface of the catalyst and a reaction occurs then the desorption process forms methyl esters product (Figure 10).

3.4. Physicochemical properties of biodiesel

To be a suitable substitute of fossil diesel, biodiesel should comply with the international standards set by the American Society for Testing Materials (ASTM). Table 1 lists the selected properties of biodiesel obtained using cellulose@α-Fe_2O_3–ZrO_2 as a catalyst. The biodiesel was a slightly yellowish liquid with properties either compliant (water content, flash point, density, kinematic viscosity, acid number, cetane number, and American petroleum institute) very close to the required values ASTM standards. The higher heating value of the produced biodiesel was comparable to that reported in previous studies [49].

3.5. Reusability of the cellulose @α-Fe_2O_3–ZrO_2 nanocomposite

When cellulose @α-Fe_2O_3–ZrO_2 was sequentially used five times for biodiesel production, the yield did not significantly change, decreasing from 92.50 of first cycle to 80.0% of fifth cycle (Figure 11). Decreasing of the product may be caused by deactivation of catalysts by product species adsorption and the unreacted lauric acid onto the surface of catalysts that could block the active sites [50].

Table 1. Physicochemical properties of biodiesel obtained in this work.

Parameters	Biodiesel product	ASTM 6751
Water content (mg kg^{-1})	0.031	<0.05
Flash point (°C)	135	>93
Density (g cm^{-3}) at 25 °C	0.853	0.85–0.90
Kinematic viscosity (mm^2 s^{-1}) at 40 °C	4.20	1.00–6.00
Acid number (mg_{KOH} g^{-1})	0.15	<0.50
Cetane number	65.00	>47
American petroleum institute	34.48	36.95
Higher heating value (MJ kg^{-1})	40.10	Not specified

The leaching of species into the reaction medium causes contamination of the product and also leads to a decrease in catalyst activity. Thus, we tested the catalytic heterogeneity of the reaction by gravimetry. The results of these studies showed that the weight of catalyst reused after five cycles is obtained constant (initial weight of 0.2 g for the first cycle until after the fifth cycle remains 0.2 g). These results demonstrated that the catalytic system behave a heterogeneous.

The results of this study suggest that the strategy of using nanocellulose in combination with α-$Fe_2O_3ZrO_2$ composites for highly efficient biodiesel production can be recoverable and reusable in biodiesel synthesis from free fatty acids sourced from coconut oil which is easily available and renewable.

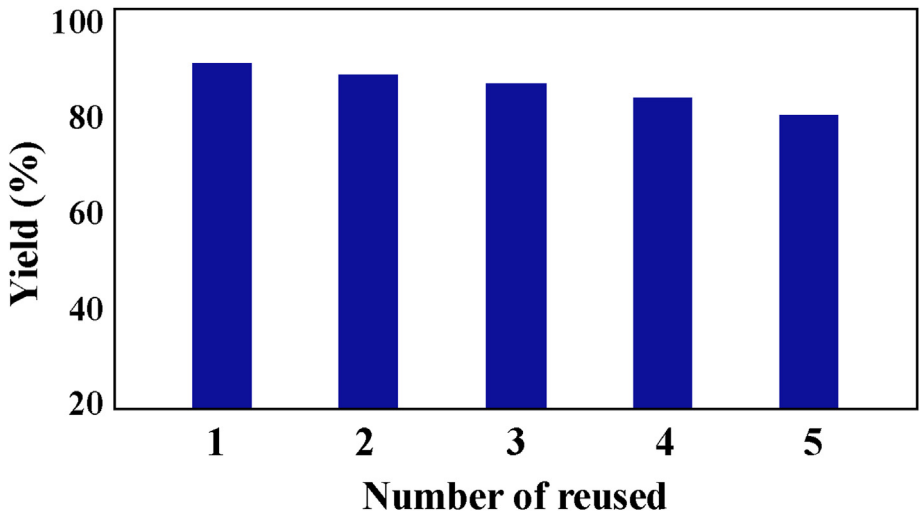

Figure 11. Nanocomposite reusability.

4. Conclusions

Herein, we report a nanocomposite derived from rice straw cellulose embedded hematite, and zirconia as a heterogeneous green catalyst for the highly efficient synthesis of biodiesel through the esterification of lauric acid with methanol. This catalyst was shown to comprise porous and irregularly shaped α-Fe_2O_3–ZrO_2 particles evenly distributed in the nanocellulose support. The presence of nanocellulose was important role for improving high catalytic activity for biodiesel production. The optimal cellulose@α-Fe_2O_3–ZrO_2 nanocomposite (nanocellulose:α-Fe_2O_3–ZrO_2 mass ratio = 2:1) achieved a biodiesel yield of 92.50%, and the properties of the obtained biodiesel were close to those stipulated by international standards. Moreover, the developed catalyst could be reused for five times without any significant activity loss.

Declarations

Author contribution statement

Helmiyati Helmiyati: Conceived and designed the experiments; Performed the experiments; Analyzed and interpreted the data; Contributed reagents, materials, analysis tools or data; Wrote the paper.

Yuni Budiman: Performed the experiments; Analyzed and interpreted the data; Wrote the paper.

Gusma Harfiana Abbas: Contributed reagents, materials, analysis tools or data.

Fitriyah Wulan Dini: Performed the experiments; Analyzed and interpreted the data.

Munawar Khalil: Conceived and designed the experiments; Analyzed and interpreted the data; Wrote the paper.

Funding statement

This work was supported by the Ministry of Research and Technology, Republic of Indonesia through the PDUPT Grant (NKB 211/UN2.RST/HKP.05.00/2020).

Data availability statement

Data included in article/supplementary material/referenced in article.

Declaration of interests statement

The authors declare no conflict of interest.

Additional information

No additional information is available for this paper.

References

[1] R.M. Moawia, M.M. Nasef, N.H. Mohamed, A. Ripin, M. Zakeri, Biopolymer catalyst for biodiesel production by functionalisation of radiation grafted flax fibres with diethylamine under optimised conditions, Radiat. Phys. Chem. (2019) 164.

[2] P. Kanmani, J. Aravind, M. Kamaraj, P. Sureshbabu, S. Karthikeyan, Environmental applications of chitosan and cellulosic biopolymers: a comprehensive outlook, Bioresour. Technol. 242 (2017) 295–303.

[3] Y. Zhao, C. Moser, M.E. Lindström, G. Henriksson, J. Li, Cellulose nanofibers from softwood, hardwood, and tunicate: preparation-structure-film performance interrelation, ACS Appl. Mater. Interfaces 9 (2017) 13508–13519.

[4] A.F. Tarchoun, D. Trache, T.M. Klapötke, B. Krumm, K. Khimeche, A. Mezroua, A promising energetic biopolymer based on azide-functionalized microcrystalline cellulose: synthesis and characterization, Carbohydr. Polym. (2020) 249.

[5] M. Krishania, V. Kumar, R.S. Sangwan, Integrated approach for extraction of xylose, cellulose, lignin and silica from rice straw, Biores. Technol. Rep. 1 (2018) 89–93.

[6] K. Xu, C. Liu, K. Kang, Z. Zheng, S. Wang, Z. Tang, W. Yang, Isolation of nanocrystalline cellulose from rice straw and preparation of its biocomposites with chitosan: physicochemical characterization and evaluation of interfacial compatibility, Compos. Sci. Technol. 154 (2018) 8–17.

[7] A. Abraham, A.K. Mathew, R. Sindhu, A. Pandey, P. Binod, Potential of rice straw for bio-refining: an overview, Bioresour. Technol. 215 (2016) 29–36.

[8] S. Tang, Q. Dong, Z. Fang, W. jie Cong, Z. diao Miao, High-concentrated substrate enzymatic hydrolysis of pretreated rice straw with glycerol and aluminum chloride at low cellulase loadings, Bioresour. Technol. (2019) 294.

[9] L. Xin, Z. Guo, X. Xiao, W. Xu, R. Geng, W. Wang, Feasibility of anaerobic digestion for contaminated rice straw inoculated with waste activated sludge, Bioresour. Technol. 266 (2018) 45–50.

[10] M. Boonterm, S. Sunyadeth, S. Dedpakdee, P. Athichalinthorn, S. Patcharaphun, R. Mungkung, R. Techapiesancharoenkij, Characterization and comparison of cellulose fiber extraction from rice straw by chemical treatment and thermal steam explosion, J. Clean. Prod. 134 (2016) 592–599.

[11] D. Kaur, N.K. Bhardwaj, R.K. Lohchab, Prospects of rice straw as a raw material for paper making, Waste Manag. 60 (2017) 127–139.

[12] V. Kandathil, M. Kempasiddaiah, S.B. S, S.A. Patil, From agriculture residue to catalyst support; A green and sustainable cellulose-based dip catalyst for C–C coupling and direct arylation, Carbohydr. Polym. (2019) 223.

[13] Y. Anggraini Helmiyati, Nanocomposites comprising cellulose and nanomagnetite as heterogeneous catalysts for the synthesis of biodiesel from oleic acid, Int. J. Techn. 10 (2019) 798–807.

[14] M.R. Santos, M.V.R. Rodrigues, A.B.S. Santos, M.G. Valerio, G.B.C. Martins, R.R. Sucupira, L. Meneghetti, P.A.Z. Suarez, Metal-cellulose catalytic systems for biodiesel preparation and reductive stabilization, J. Mol. Catal. Chem. 422 (2016) 131–141.

[15] A. Maleki, V. Eskandarpour, J. Rahimi, N. Hamidi, Cellulose matrix embedded copper decorated magnetic bionanocomposite as a green catalyst in the synthesis of dihydropyridines and polyhydroquinolines, Carbohydr. Polym. 208 (2019) 251–260.

[16] S.B. Khan, K.A. Alamry, H.M. Marwani, A.M. Asiri, M.M. Rahman, Synthesis and environmental applications of cellulose/ZrO2 nanohybrid as a selective adsorbent for nickel ion, Compos. B Eng. 50 (2013) 253–258.

[17] X. Yu, S. Tong, M. Ge, J. Zuo, C. Cao, W. Song, One-step synthesis of magnetic composites of cellulose@iron oxide nanoparticles for arsenic removal, J. Mater. Chem. 1 (2013) 959–965.

[18] M.E. Günay, L. Türker, N.A. Tapan, Significant parameters and technological advancements in biodiesel production systems, Fuel 250 (2019) 27–41.
[19] Helmiyati, G.H. Abbas, Y. Budiman, S. Ramadhani, Synthesis of MgFe2O4-MgO nanocomposite: influence of MgO on the catalytic activity of magnesium ferrite in biodiesel production, Rasayan J. Chem. 13 (2020) 298–305.
[20] M. Anwar, M.G. Rasul, N. Ashwath, The efficacy of multiple-criteria design matrix for biodiesel feedstock selection, Energ. Convers. Manag. (2019) 198.
[21] M.L. Savaliya, B.Z. Dholakiya, Eco-friendly process for preparation of biodiesel from WFO over MTSA-Si catalyst: an innovative approach for the utilization of side product, J. Ind. Eng. Chem. 64 (2018) 352–366.
[22] M.S. Dhawan, G.D. Yadav, Insight into a catalytic process for simultaneous production of biodiesel and glycerol carbonate from triglycerides, Catal. Today 309 (2018) 161–171.
[23] Shobhana-Gnanaserkhar, N. Asikin-Mijan, G. AbdulKareem-Alsultan, Sivasangar-Seenivasagam, S.M. Izham, Y.H. Taufiq-Yap, Biodiesel production via simultaneous esterification and transesterification of chicken fat oil by mesoporous sulfated Ce supported activated carbon, Biomass Bioenergy 141 (2020).
[24] M.J. Borah, A. Das, V. Das, N. Bhuyan, D. Deka, Transesterification of waste cooking oil for biodiesel production catalyzed by Zn substituted waste egg shell derived CaO nanocatalyst, Fuel 242 (2019) 345–354.
[25] Y. Putrasari, A. Praptijanto, W.B. Santoso, O. Lim, Resources, policy, and research activities of biofuel in Indonesia: a review, Energy Rep. 2 (2016) 237–245.
[26] Y.Z. Han, L. Hong, X.Q. Wang, J.Z. Liu, J. Jiao, M. Luo, Y.J. Fu, Biodiesel production from Pistacia chinensis seed oil via transesterification using recyclable magnetic cellulose-based catalyst, Ind. Crop. Prod. 89 (2016) 332–338.
[27] H. Helmiyati, R.P. Suci, Nanocomposite of cellulose-ZnO/SiO2 as catalyst biodiesel methyl ester from virgin coconut oil, in: AIP Conference Proceedings, American Institute of Physics Inc., 2019.
[28] P. Lu, Y. lo Hsieh, Preparation and characterization of cellulose nanocrystals from rice straw, Carbohydr. Polym. 87 (2012) 564–573.
[29] K.S. Prado, M.A.S. Spinacé, Isolation and characterization of cellulose nanocrystals from pineapple crown waste and their potential uses, Int. J. Biol. Macromol. 122 (2019) 410–416.
[30] E. Darezereshki, F. Bakhtiari, M. Alizadeh, A. Behrad Vakylabad, M. Ranjbar, Direct thermal decomposition synthesis and characterization of hematite (α-Fe 2O 3) nanoparticles, Mater. Sci. Semicond. Process. 15 (2012) 91–97.
[31] C.R. Chintaparty, Influence of calcination temperature on structural, optical, dielectric properties of nano zirconium oxide, Optik 127 (2016) 4889–4893.
[32] C. Feng, C. Aldrich, J.J. Eksteen, D.W.M. Arrigan, Removal of arsenic from alkaline process waters of gold cyanidation by use of γ-Fe2O3@ZrO2 nanosorbents, Hydrometallurgy 174 (2017) 71–77.
[33] M.H. Beyki, M.H. Ghasemi, Quaternized γ-Fe2O3@cellulose ionomer: an efficient recyclable catalyst for Michael-type addition reaction, Int. J. Biol. Macromol. 113 (2018) 711–718.
[34] L. Zhou, R. Yarra, H. Cao, SSR based association mapping analysis for fatty acid content in coconut flesh and exploration of the elite alleles in Cocos nucifera L, Curr. Plant Biol. 21 (2020).
[35] A.M. El-Nahas, T.A. Salaheldin, T. Zaki, H.H. El-Maghrabi, A.M. Marie, S.M. Morsy, N.K. Allam, Functionalized cellulose-magnetite nanocomposite catalysts for efficient biodiesel production, Chem. Eng. J. 322 (2017) 167–180.
[36] H.R. Harsha Hebbar, M.C. Math, K.v. Yatish, Optimization and kinetic study of CaO nano-particles catalyzed biodiesel production from Bombax ceiba oil, Energy 143 (2018) 25–34.
[37] A.J. Folayan, P.A.L. Anawe, A.E. Aladejare, A.O. Ayeni, Experimental investigation of the effect of fatty acids configuration, chain length, branching and degree of unsaturation on biodiesel fuel properties obtained from lauric oils, high-oleic and high-linoleic vegetable oil biomass, Energy Rep. 5 (2019) 793–806.
[38] A.S. Yusuff, A.K. Bhonsle, J. Trivedi, D.P. Bangwal, L.P. Singh, N. Atray, Synthesis and characterization of coal fly ash supported zinc oxide catalyst for biodiesel production using used cooking oil as feed, Renew. Energy 170 (2021) 302–314.
[39] T.F. Adepoju, B.E. Olatunbosun, O.M. Olatunji, M.A. Ibeh, Brette Pearl Spar Mable (BPSM): a potential recoverable catalyst as a renewable source of biodiesel from Thevetia peruviana seed oil for the benefit of sustainable development in West Africa, Energy, Sustainabil. Soci. 8 (2018).
[40] M.A. Sundaramahalingam, S. Karthikumar, R. Shyam Kumar, K.J. Samuel, S. Shajahan, V. Sivasubramanian, P. Sivashanmugam, P. Varalakshmi, A. Syed, N. Marraiki, A.M. Elgorban, R. Vinoth Kumar, I. Ganesh Moorthy, An intensified approach for transesterification of biodiesel from Annona squamosa seed oil using ultrasound-assisted homogeneous catalysis reaction and its process optimization, Fuel 291 (2021).
[41] S.I. Akinfalabi, U. Rashid, C. Ngamcharussrivichai, I.A. Nehdi, Synthesis of reusable biobased nano-catalyst from waste sugarcane bagasse for biodiesel production, Environ. Techn. Innov. 18 (2020).
[42] A.S. Abou-Elyazed, G. Ye, Y. Sun, A.M. El-Nahas, A series of UiO-66(Zr)-Structured materials with defects as heterogeneous catalysts for biodiesel production, Ind. Eng. Chem. Res. 58 (2019) 21961–21971.
[43] H. Helmiyati, I. Masriah, Preparation of cellulose/CaO-Fe2O3 nanocomposites as catalyst for fatty acid methyl ester production, in: AIP Conference Proceedings, American Institute of Physics Inc., 2019.
[44] M. Tadic, D. Trpkov, L. Kopanja, S. Vojnovic, M. Panjan, Hydrothermal synthesis of hematite (α-Fe2O3) nanoparticle forms: synthesis conditions, structure, particle shape analysis, cytotoxicity and magnetic properties, J. Alloys Compd. 792 (2019) 599–609.
[45] A. Parveen, N. Surumbarkuzhali, Spatial separation of photo-generated carriers and enhanced photocatalytic performance on ZrO2 catalysts via coupling with PPy, Inorg. Chem. Commun. 120 (2020).
[46] T. Zhong, R. Dhandapani, D. Liang, J. Wang, M.P. Wolcott, D. van Fossen, H. Liu, Nanocellulose from recycled indigo-dyed denim fabric and its application in composite films, Carbohydr. Polym. 240 (2020) 116283.
[47] A. Benhammada, D. Trache, M. Kesraoui, A.F. Tarchoun, S. Chelouche, A. Mezroua, Synthesis and characterization of α-Fe2O3 nanoparticles from different precursors and their catalytic effect on the thermal decomposition of nitrocellulose, Thermochim. Acta 686 (2020).
[48] P.A. Monson, Understanding adsorption/desorption hysteresis for fluids in mesoporous materials using simple molecular models and classical density functional theory, Microporous Mesoporous Mater. 160 (2012) 47–66.
[49] B. Nath, P. Kalita, B. Das, S. Basumatary, Highly efficient renewable heterogeneous base catalyst derived from waste Sesamum indicum plant for synthesis of biodiesel, Renew. Energy 151 (2020) 295–310.
[50] A.S. Abou-Elyazed, Y. Sun, A.M. El-Nahas, A.M. Yousif, A green approach for enhancing the hydrophobicity of UiO-66(Zr) catalysts for biodiesel production at 298 K, RSC Adv. 10 (2020) 41283–41295.